Wear xxx (xxxx) xxx

Contents lists available at ScienceDirect

Wear

journal homepage: http://www.elsevier.com/locate/wear

A study of influence of hydraulic pressure on micro-hydromechanical deep drawing considering size effects and surface roughness

Liang Luo [a,*], Zhengyi Jiang [b], Dongbin Wei [c], Fanghui Jia [b]

[a] Automotive Research Institute, Hefei University of Technology, Hefei, Anhui, 230009, China
[b] School of Mechanical, Materials, Mechatronic and Biomedical Engineering, University of Wollongong, Wollongong, NSW, 2522, Australia
[c] School of School of Mechanical and Mechatronic Engineering, University of Technology Sydney, Sydney, NSW, 2007, Australia

ARTICLE INFO

Keywords:
Micro-hydromechanical deep drawing
FSI
Size effects
Surface roughness
Micro-forming

ABSTRACT

Micro-hydromechanical deep drawing (MHDD) is a promising micro-manufacturing technology to fabricate micro-metallic products in batch scale. Size effects significantly affect MHDD regarding both material properties and friction. Hydraulic pressure on the blank and its development differ from that in conventional hydromechanical deep drawing. Combined influence of fluid pressure, surface roughness and material inhomogeneity of the blank was investigated in this study via MHDD experiments and advanced FE simulation considering strong fluid-solid interaction (FSI) and size effects. The MHDD experiments under different hydraulic pressures were conducted using the annealed foil followed by the advanced FE simulation. The foil can be successfully drawn into micro-cups, however, wrinkles occurred under high hydraulic pressures. Wrinkle height and number are affected by hydraulic pressure and size effects. Average hydraulic pressure on the blank is lower than the inlet pressure, and pressure development on the blank depends on location and is complex, due to transition of sealing between the blank and die. The maximum drawing force increases, while the contact forces and pressures on the blank holder and die decrease with an increase of hydraulic pressure. Optimal hydraulic pressure for MHDD should be determined with consideration of size effects and MHDD tool geometry.

1. Introduction

Micro-silicon products have been widely applied in micro-electromechanical systems (MEMS) and micro-system technology (MST). Increasing micro-product market urgently requires micro-metallic products with advantages of high-aspect ratio, high strength, and good anti-corrosion and thermal performances. These advantages expand micro-metallic product's applications in MEMS, MST, optical, telecommunication, transportation and medical fields [1,2]. Micro-forming that handles materials with at least two dimensions in microscale owns batch production potential, and heritages advantage of (near) net manufacturing of metal forming [3]. Additionally, relatively low requirements on operators and economical micro-forming tools enable micro-forming to be a promising micro-metal manufacturing technology compared with other micro-manufacturing technologies [4].

Due to reduced sizes, size effects become obvious and significantly affect micro-forming processes [5]. Increased friction coefficient was experimentally observed in different micro-forming experiments and explained by the open-closed lubricant pockets theory which has been proved in micro-foil forming experiments [6–8]. Friction coefficient scatters under different drawing conditions, and can be described as pressure-dependent [9] and contact-length dependent functions [10]. Friction force accounts a larger portion of total forming force in micro-forming [11]. Surface roughness shows an impact on influence of friction size effect [12]. Positioning of micro-deep drawing (MDD) tool significantly affects the tool's wear behaviour [13]. Diamond-like carbon (DLC) coating can more effectively reduce required drawing force than usual lubricant in MDD [14]. Moreover, material deformation behaviour differs from that in conventional scale. An individual grain plays an important role in deformation behaviour of a sample in microscale and the micro-sample presents inhomogeneous properties [15,16]. Material constitutive model established in conventional scale cannot accurately predict deformation behaviour in microscale, and thus variously models taken feature size and metallurgical characteristics of a micro-sample into account were developed [5,17].

MDD is a typical micro-forming technology and its micro-hollow products are widely used micro-metallic products [18,19]. An increasing drawing ratio and more complex shapes of the micro-cups are

* Corresponding author.
E-mail address: Liang_LUO@hfut.edu.cn (L. Luo).

https://doi.org/10.1016/j.wear.2021.203803
Received 31 August 2020; Received in revised form 4 January 2021; Accepted 3 February 2021
Available online 10 March 2021

constantly required [20]. Thus, MHDD that applies counter pressure on opposite side of a blank to the punch is introduced to draw advantage of fluid pressure for further improvement of MDD process [21]. Hydraulic pressure is important to wrinkling in both conventional and micro-hydromechanical deep drawing. Neither a too high nor a too low pressure will result in wrinkles [22]. Wrinkle wave height can be reduced by 76% under high back pressure [23]. Critical hydraulic pressure to avoid wrinkles during MHDD should be based on foil's initial yield stress [19]. Fluid acts as lubricant and reduces friction in MHDD [24]. Furthermore, pressured fluid presses the blank to hold the punch and improves blank holding effect which benefits the drawing process [25]. Over pressed fluid, by contrast, leads to fracture of drawn cups [11]. Therefore, proper fluid pressure is vital important to MHDD. The hydraulic pressure is generally assumed evenly distributed on the blank in conventional hydromechanical deep drawing. The pressure in MHDD, however, is timely changeable and shows high pressure gradient. MHDD with radial pressure was developed to improve lubrication effect [25]. Micro-pneumatic deep drawing was developed to draw micro-cups at elevated temperatures [26]. Nano-particle added lubricant was used in MDD to reduce required drawing force [27]. Grain size and feature size affect required hydraulic pressure to produce single polar plates [28]. Forming limit and dimensional accuracy were improved in MHDD experiments with different metal foils [21]. Hydraulic pressure helps to reduce oxide film peeling from the foil [29], and affects wrinkling and earing of drawn cups [30].

In this study, the fluid development and pressure distribution on the blank were investigated, and their influence on MHDD was analysed. Firstly, MHDD experiments under different hydraulic pressures were conducted. Next, a FSI FE model with consideration of blank surface morphology and material inhomogeneity was built. Both experimental and numerical results were then compared and analysed, followed by the conclusions.

2. Materials and experiments

The stainless steel SUS304 foil with a nominal thickness of 50 μm was firstly annealed at 975 °C for 2 min following a heat treatment route shown in Fig. 1(a), in a tube furnace with argon gas protective ambience. After the heat treatment, the foil was observed under a KEYENCE VK-X1000/X2000 3D laser confocal microscope and microstructure of the annealed foil is shown in Fig. 5(a). Next, 10 times micro-tensile tests were performed using the annealed foil in order to obtain material properties. The results are shown in Fig. 1(b) in which mean value and scatter range are displayed.

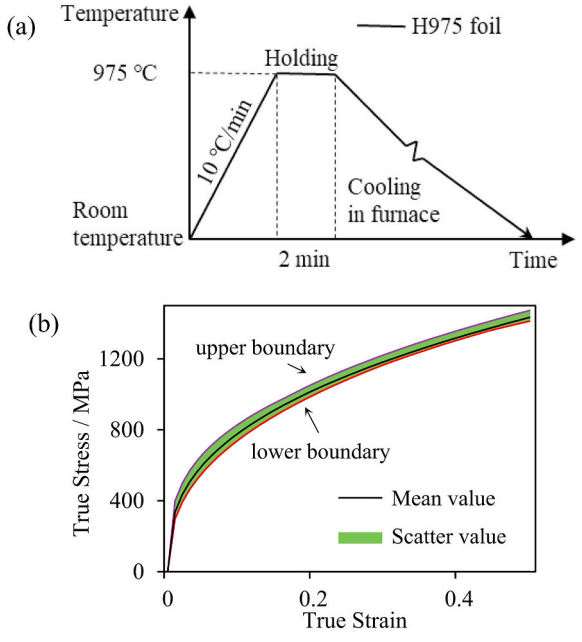

Fig. 1. (a) Heat treatment route of the SUS304 foil and (b) true stress-strain curve obtained from the micro-tensile tests.

MHDD experiments were conducted under different hydraulic pressures using a MHDD system. The MHDD system consists of a hydraulic system (Fig. 2(a)) providing hydraulic pressure and a modified MDD system (Fig. 2(b)) with a fluid inlet at bottom of the die. Geometry of the MHDD tools are shown in Fig. 2(c). The #46 hydraulic oil with was used as lubricant. Moreover, the hydraulic system supplied hydraulic pressure from 5 MPa to 30 MPa at an interval increment of 5 MPa. Under each hydraulic pressure, 5 times repeated MHDD experiments were performed in order to reflect size effects. The drawing speed was 0.1 mm/s and the blank holder-die gap was constantly 55 μm in all the experiments. The foil and drawn cups were cleaned by ultrasonic vibration in alcohol. MHDD tools were also cleaned by alcohol before each experiment. The drawn cups were observed by the KEYENCE VK-X1000/X2000 3D laser confocal microscope. The MDD experiments without hydraulic pressure support were also conducted as a comparison with the MHDD experiments.

3. Advanced FE models

A preliminary MDD FE model was firstly developed in LS-DYNA and the model had the same size of the MHDD tools. A quarter of the blank with symmetrical boundaries was modelled to accelerate computing speed. Shell elements were used to mesh rigid MHDD tools (punch, die and blank holder) and the deformable blank. Full integration element model with seven integration points along thickness direction was applied. The 3-parameter-Barlat material model [31] was utilized for representing blank's deformation behaviour and the model's parameters were obtained from the micro-tensile tests results. Friction coefficient between blank and die/blank holder was 0.05 and that between blank and punch was 0.2. A drawing speed of 0.1 mm/s was assigned to the punch and a constant blank holder-die gap of 55 μm was set in the FE model.

In conventional hydromechanical deep drawing processes, an even pressure distribution on the blank is usually assumed and the pressure load depends on drawing stroke due to relatively long drawing time and easy control on hydraulic pressure. The hydraulic pressure on the blank during MHDD, however, is timely changeable and not evenly distributed due to high pressure gradient in reduced sizes. Moreover, deformation of the blank affects the development and distribution of hydraulic pressure. Therefore, two-way FSI should be considered in MHDD simulation. An arbitrary Lagrange Eulerian (ALE) model [32] that can represent FSI was built based on the preliminary MDD model and a separated fluid phase occupying vacancy of the die in a Eulerian form. The fluid is fully developed before flowing into the die in the MHDD experiments and the fluid path between the die and blank is small. Therefore, laminar flow state of the hydraulic oil in the MHDD can be assumed. Inner vacant volume of the die was initially filled with the pressed oil and modelled with fully hexahedral meshes. Furthermore, a layer of mesh at bottom of the fluid phase was set as pressure inlet with an assigned pressure value and a top layer was set as pressure outlet under an atmospheric pressure as shown in Fig. 3(b). Fluid development followed a linear polynomial equation of state (EOS) as shown in Eq. (1), with initial density of 0.9×10^3 kg/m^3 and a constant viscosity of 46 cSt. The penalty method was used to fulfil interaction between the blank and the oil. One surface of the blank facing the oil was set as an interface where fluid pressure transfers to the blank via calculated penalty force. The fluid volume was set as a multi-material group so that blank and fluid can exist in one mesh element simultaneously. During the simulation, The MDD model and fluid model run alternatively, and a process of remeshing of fluid mesh and transferring of data between the two phases was conducted between the MDD and fluid calculation cycles.

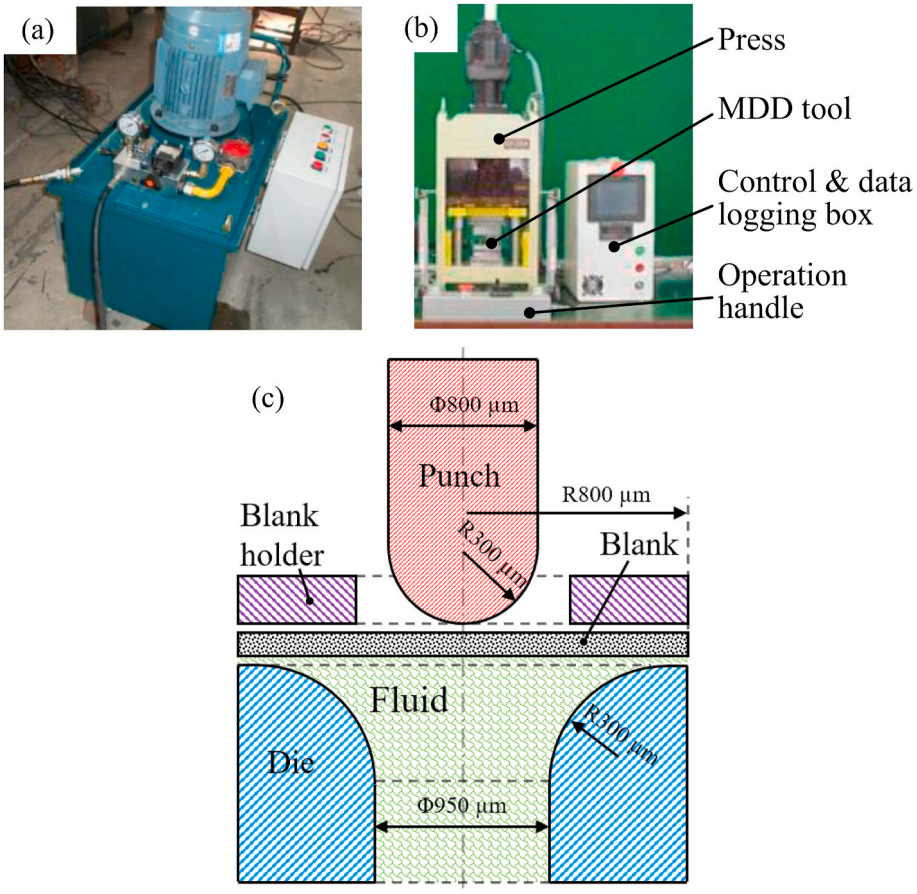

Fig. 2. MHDD system including (a) the hydraulic station and (b) the modified MDD system; (c) geometry of the MHDD tools.

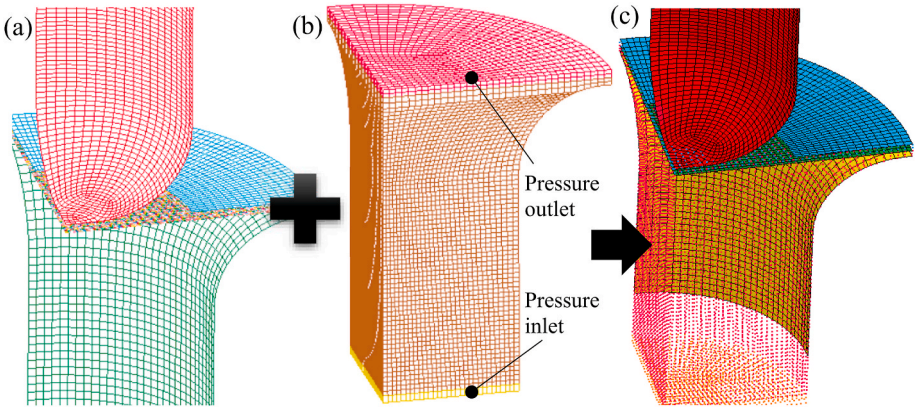

Fig. 3. Developed MHDD model: (a) solid phase (MDD model), (b) fluid phase and (c) whole ALE model.

$$p = C_0 + C_1\mu + C_2\mu^2 + C_3\mu^3 + \left(C_4 + C_5\mu + C_6\mu^2\right)E \quad (1)$$

where p is hydraulic pressure, $C_{i=0,1,2,\ldots,6}$ is EOS coefficients, E is internal energy per unit reference volume, and μ is relative density change.

Size effects need to be considered in micro-forming simulation [33]. In order to reflect the material and friction size effects, the blank FE model was further modified. Shell thickness was changed to mimic blank's surface morphology. The blank's FE model document in '*keyword' format, including elemental and nodal information, and foil's surface morphology digital information obtained by the microscope were firstly imported into MATLAB. Next, based on a calibration factor calculated from the scale bar, the FE model was mapped on the foil surface. Each node's thickness was modified according to its corresponding asperity height on the foil surface. Fig. 4 shows the observed surface morphology of the foil and its corresponding surface morphology model. The surface asperities represented as various shell thicknesses will result in differently local contact in LS-DYNA according to the penalty contact algorithm.

Inhomogeneious material properties of the blank were modelled on micro-scale. The microstructure image of the foil was imported into MATLAB and grain boundaries were identified via the developed image processing program. The blank FE model with detailed '*part' information was imported into MATLAB and mapped on the microstructure image based on the calibration factor. Each element was set its own material model according to the relation between the element and

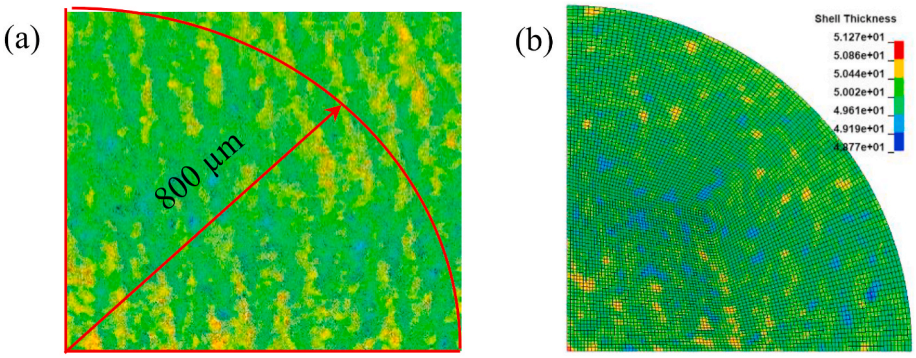

Fig. 4. (a) Surface morphology of the foil and (b) its corresponding surface roughness blank FE model.

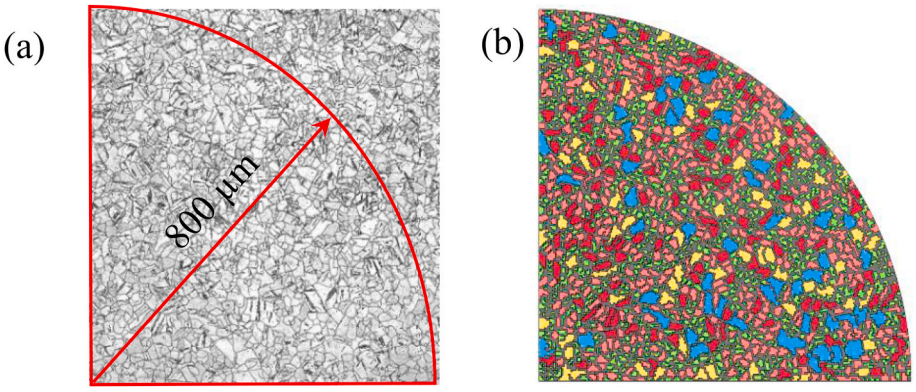

Fig. 5. (a) Foil's microstructure after heat treatment and (b) its corresponding material heterogeneity blank FE model.

identified grains and grain boundaries. Fig. 5 shows the microstructure of the foil and its corresponding heterogeneity blank FE model in which different colours represent different material models with different material parameters. The material parameters were calculated based on the micro-tensile test results shown in Fig. 1(b).

The preliminary blank model in the ALE model was than replaced by the developed advanced blank model. Thus, the developed model can consider FSI, material heterogeneity and surface morphology. Modelling sequence regarding FSI, material heterogeneity and surface roughens dose not influence simulation results as each modification refers to different information of the FE model.

4. Results and analysis

4.1. Drawing force

The drawing forces in MHDD experiments under 5 MPa and 30 MPa hydraulic pressures are respectively presented on Fig. 6(a) and (b). Obvious scatter of the maximum drawing forces can be observed as a result of size effects. Moreover, under low pressures, such as 5 MPa and 10 MPa, there was only one peak of a drawing force curve. By contrast, there were two local peaks when the foil was drawn under high pressures. The dual peaks indicate wrinkles occurred during MHDD, which can be observed on the drawn cups shown in Fig. 11. Additionally, the first peak occurred at about moment when the blank leaves from the blank holder. Due to random occurrence and height of wrinkles, the time when the blank leaves the blank holder differs, and the first peaks show obvious difference regarding time and value. High hydraulic pressure leads to pre-bulging and the blank is bulged in reverse direction of drawing before the punch's movement. This pre-bulging alters strain-stress development of the blank, and triggers wrinkling resulting additional first peak drawing force. The inappropriate hydraulic pressure triggers and increases compression instability of the blank. The wrinkles were drawn into the die, which further affects blank-die friction and the drawing force. Additionally, due to integrated effect of hydraulic pressure and size effects, the blank randomly wrinkled regarding locations, number and height of wrinkles on the drawn cup. The randomness of the wrinkles signified scatter of the maximum drawing force regarding the force value and onset time. Slopes of the drawing forces in early drawing stage under low hydraulic pressures was smooth and turned sharp in the later drawing stage. By contrast, the slopes kept sharp till reaching the maximum drawing force when high hydraulic pressures were applied. This difference indicates different strain-stress state of the foil drawn under different hydraulic pressures. Thus, a high pressure that greatly pre-bulges blank and affect strain-stress state of the blank will introduce wrinkles and cause dual peaks of the drawing force. As the maximum drawing force strongly related to drawability, the maximum drawing force was compared and shown in Fig. 6(c). The developed advanced FE simulation predicted accurate maximum drawing forces compared with the experimental results.

4.2. Pressure development

The hydraulic pressure development on the blank was successfully presented by the advanced FE model. The average hydraulic pressure on the blank was generally lower than the inlet pressure, and high inlet pressure resulted in high average hydraulic pressure on the blank, as illustrated on Fig. 7(a). Furthermore, pressure developments on different locations of the blank were different. The pressure on blank edge area was quite low regardless of the inlet pressure, while that on centre of the blank was constantly high and close to the inlet pressure. The pressure on the blank contacting with punch corner area presented complex development, as shown in Fig. 7(b). This complex hydraulic pressure development can be explained by change of sealing between

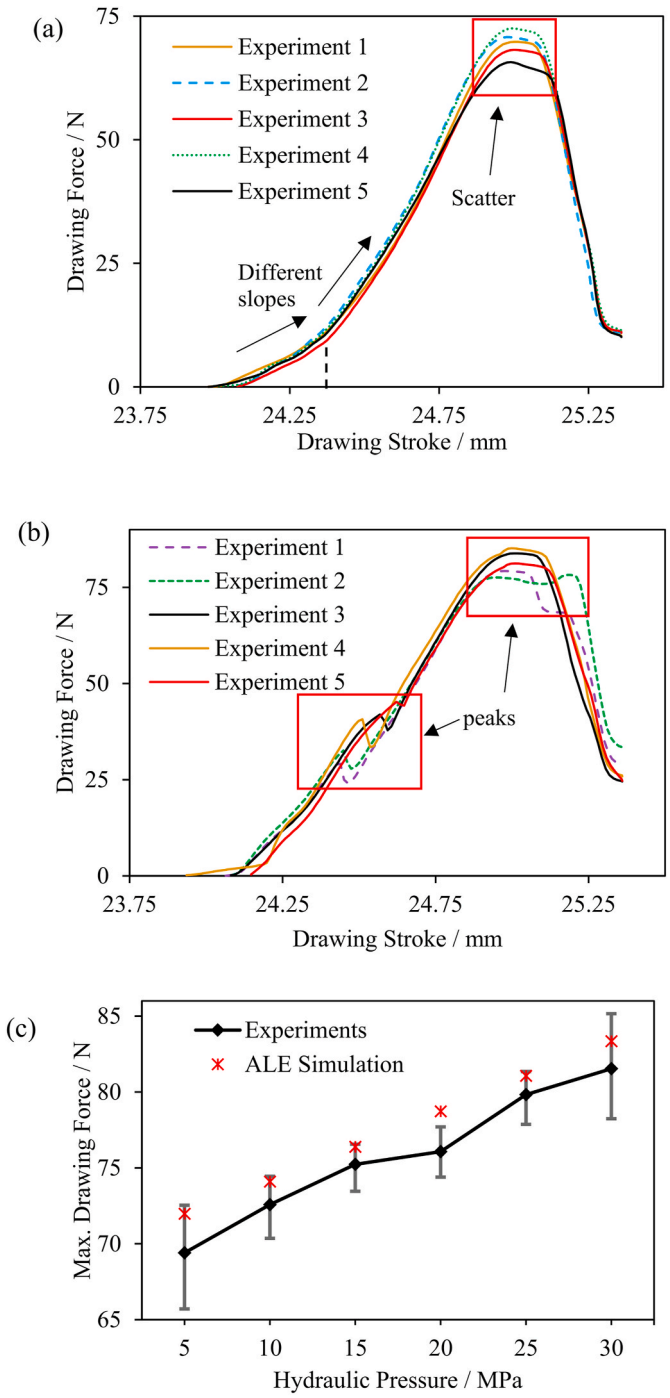

Fig. 6. Drawing forces of the MHDD experiments under hydraulic pressures of: (a) 5 MPa and (b) 30 MPa; and (c) comparison of the maximum drawing force between simulation and experiments under different pressures.

the blank and the die during the drawing process, as illustrated in Fig. 8. At start of the drawing process, the blank edge area was sealed and the hydraulic pressure radially inside this sealing area was high. As the blank being drawn into the die, sealing area changes from the edge to middle of the blank and from die corner to die cylindrical wall. Generally, the sealing area is the watershed of hydraulic pressure distribution. Inside of the sealing area the blank is under relatively high pressure while outer part of the blank understands low pressure. Thus, the MHDD tools geometry, particularly the die and punch geometries, significantly affect the development of the hydraulic pressure distribution on the blank.

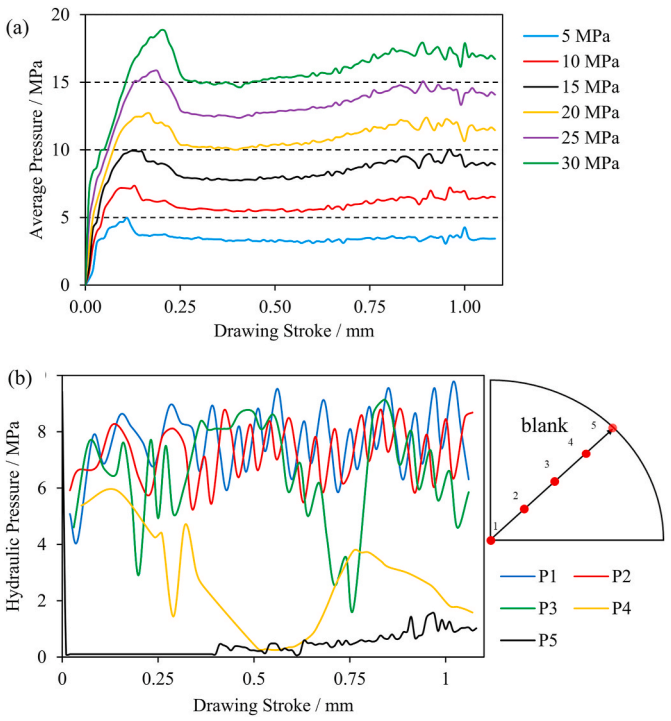

Fig. 7. (a) Average hydraulic pressure on the blank and (b) hydraulic pressure development on different positions of the blank when drawn under 10 MPa inlet hydraulic pressure.

4.3. Contacts on die and blank holder

Fig. 9(a) displays the contact forces on the blank holder when drawn under different pressures. Due to the hydraulic pressure, there were two waves of the contact force on the blank holder. Moreover, low hydraulic pressure led to low contact force on the blank holder at start while a high peak contact force in the later drawing process. At the start of drawing process, the contact force on the blank holder mainly comes from hydraulic pressure. Therefore, high inlet pressure leads to high average hydraulic pressure on the blank and high contact force on the blank holder. An early drop of the contact force was predicted under low hydraulic pressure drawing conditions. Once the blank contacts with the die, the contact on the blank holder increases. Moreover, high inlet pressure contributes to later contact with the die and later increase of the contact force on the blank holder. The hydraulic pressure signified blank holding effect and the punch withstood most of hydraulic force transferred via the blank. Therefore, the highest load on the blank holder decreased with an increase of hydraulic pressure. The contact force finally decreased to zero indicating that the blank leaves the blank holder.

The contact force on the die remained zero for a short time initially and then increased due to that hydraulic pressure separated the blank and die at start of MHDD. As shown in Fig. 7(b), the hydraulic pressure near blank edge was high initially and then decreased. At the start only blank edge area contacted with the die, therefore, contact force kept zero. After a sharp growth, the contact force stayed still for a short moment and rose again since 0.4 mm drawing stroke. The contact area of blank transferred to corner as shown in Fig. 8, and contact force rose to a peak. Thereafter, contact transferred to drawn cup side wall area and a decreasing contact force can be predicted. Moreover, the high hydraulic pressure resulted in low contact force on the die during the whole MHDD process as the average hydraulic pressure on the blank was kept high when the input pressure was high.

Uneven contact can be predicted by the advanced model under all hydraulic pressures, as displayed in Fig. 10(a~c). The maximum contact

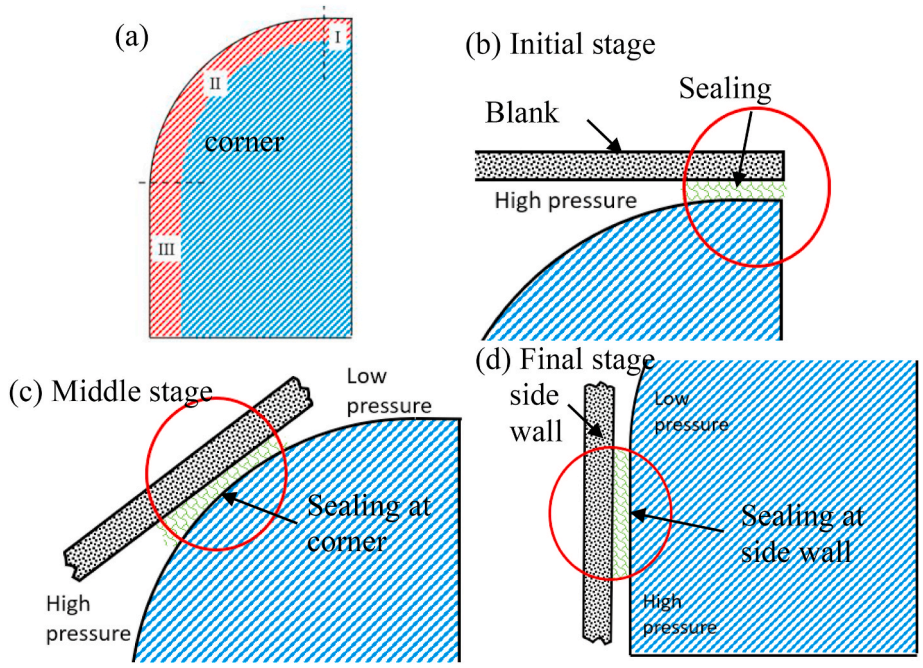

Fig. 8. (a) Three areas of the die, and different sealing areas at different drawing stages: (b) initial drawing stage when blank contact with die annular plane area (I), (c) middle drawing stage when blank contact with die corner area (II) and (d) final drawing stage when blank sliding on die cylindrical side wall area (III).

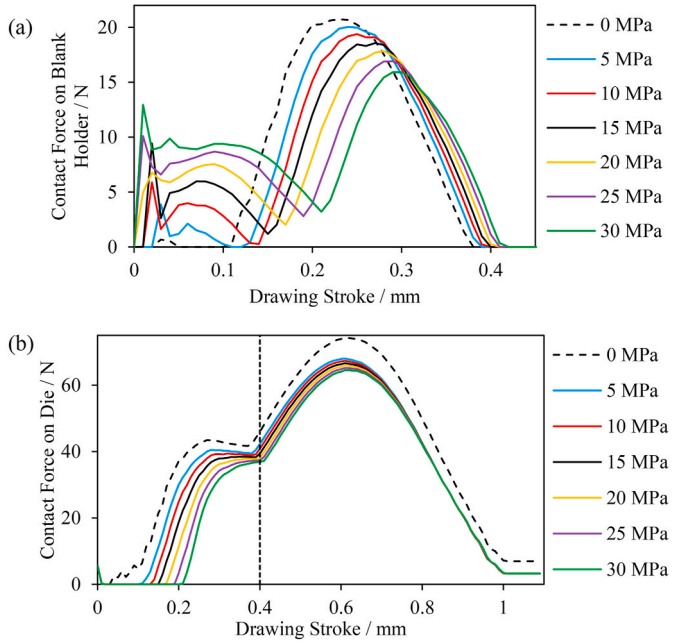

Fig. 9. Contact forces (a) between blank and blank holder and (b) between blank and die.

pressure on the die at 0.4 mm drawing stroke decreased with an increase of hydraulic pressure, as shown in Fig. 10(d). Increased hydraulic pressure also reduced the maximum contact pressure on the blank holder.

Due to the hydraulic pressure support on the blank, the contact pressure on the die decreased. The hydraulic pressure support decreased the bending diameter of blank at die corner area. The contact area between the blank and the blank holder increased and thus the contact pressure decreased.

The hydraulic pressure is beneficial to reduce the maximum contact force and the maximum contact pressure on the blank holder and die, which may improve MHDD tools service life because of reduced wear.

4.4. Drawn cups

Fig. 11 shows the drawn cups from the MHDD experiments under different hydraulic pressures. Without and with low hydraulic pressures, the drawn cups were round, and their mouths were smooth. When drawn under high pressures, winkles occurred randomly due to size effects and hydraulic pressure. Hydraulic pressure disturbed stability of the blank and caused wrinkles on weak and thin areas of the blank edge. Relationship between hydraulic pressure and wrinkles was complex due to integrated influence of size effects and hydraulic pressure [19].

An image processing program was developed in MATLAB to recognize profiles of the drawn cup mouth. Due to limitation of the die, the blank was wrinkled inwards upon the punch and the wrinkles were inside the drawn cups. Thus, the wrinkles were defined as locally radial difference of the inner profile. Fig. 12(a) illustrates the recognized drawn cup mouth profiles and Fig. 12(b) shows the wrinkle heights measured from the experimental results. The local inner profile with an inwards bulge while a smoothly corresponding outer profile is treated as thickened wall. Only both inner and outer profiles of an area showing inwards bulges is treated as a wrinkle.

$$H_{wj} = max\left\{\frac{\bar{r} - r_i}{\bar{r}} \times 100\%\right\}_j \quad (2)$$

where H_{wj} is the jth wrinkle height, $\bar{r}$ is the average profile radius and r_i is the radius of the ith point on a drawn cup mouth inner profile.

Both the number of wrinkles on a drawn cup and the defined wrinkle height were increased firstly with an increase of hydraulic pressure. With a further increase of hydraulic pressure, the wrinkle height and number were decreased. This complex relationship with hydraulic pressure is resulted from integrated effects of blank inhomogeneity, surface morphology and hydraulic pressure. The hydraulic pressure reduces contact force between blank and blank holder, and consequently constrain on compression decreases. Therefore, compression stability of the blank decreases when hydraulic pressure slightly increased. High hydraulic pressures, on the other hand, reduces blank bending radius at

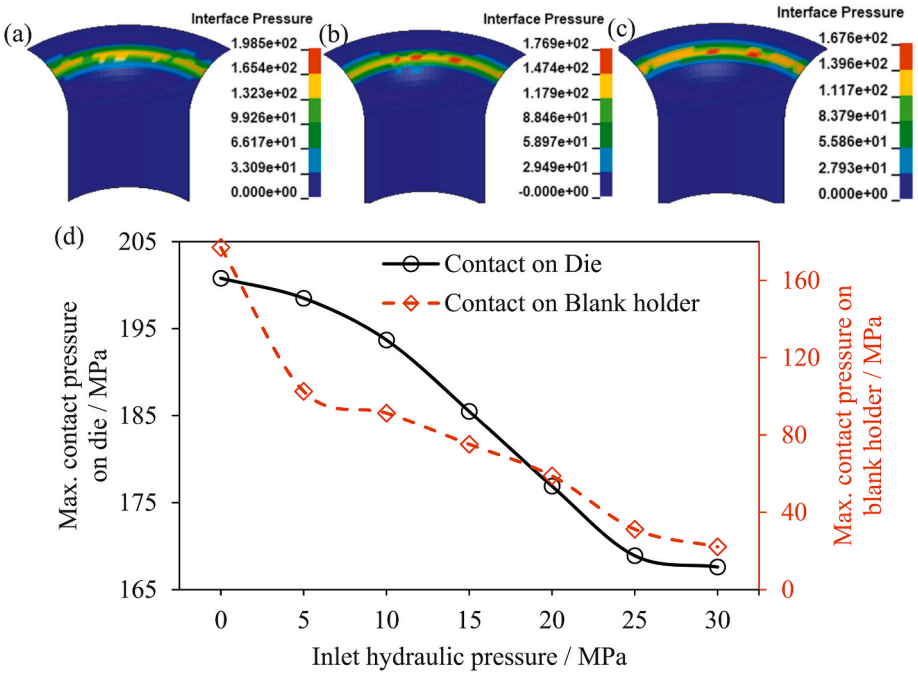

Fig. 10. Contact pressure distribution on the die at the drawing stroke of 0.4 mm under hydraulic pressures of: (a) 5 MPa, (b) 20 MPa and (c) 30 MPa; (d) the maximum contact pressure on the blank holder at drawing stroke of 0.2 mm and on the die at drawing stroke of 0.4 mm.

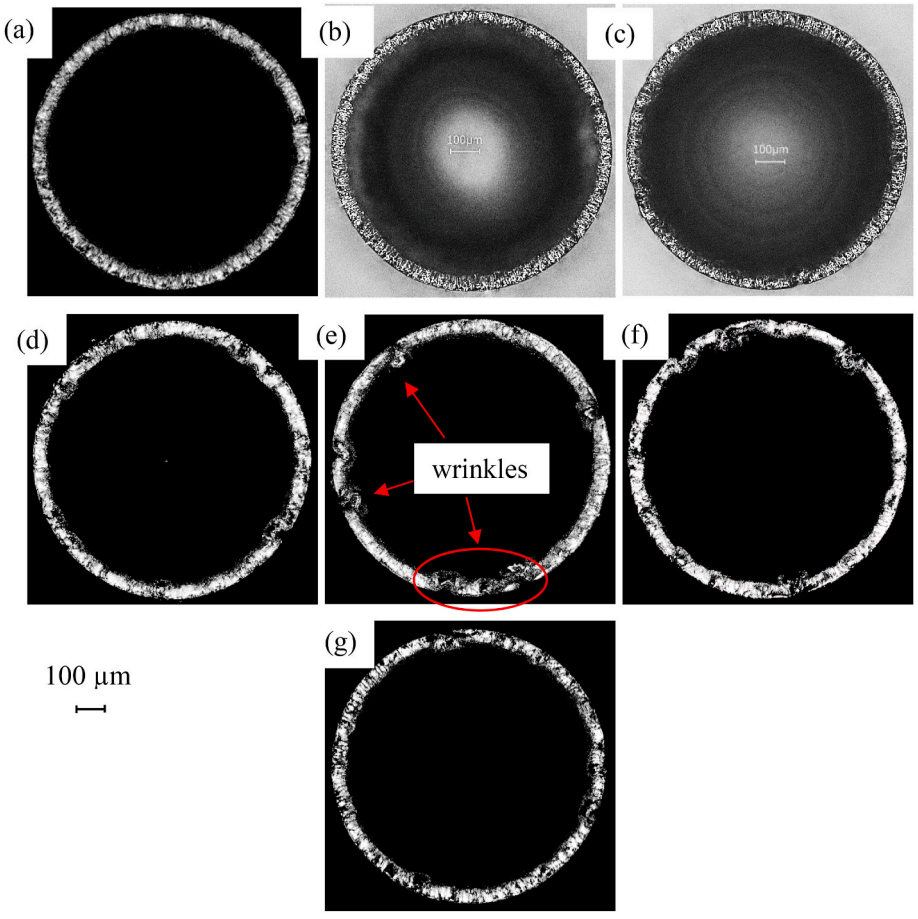

Fig. 11. Drawn cups drawn under different hydraulic pressures: (a) 0 MPa, (b) 5 MPa, (c) 10 MPa, (d) 15 MPa, (e) 20 MPa, (f) 25 MPa, and (g) 30 MPa.

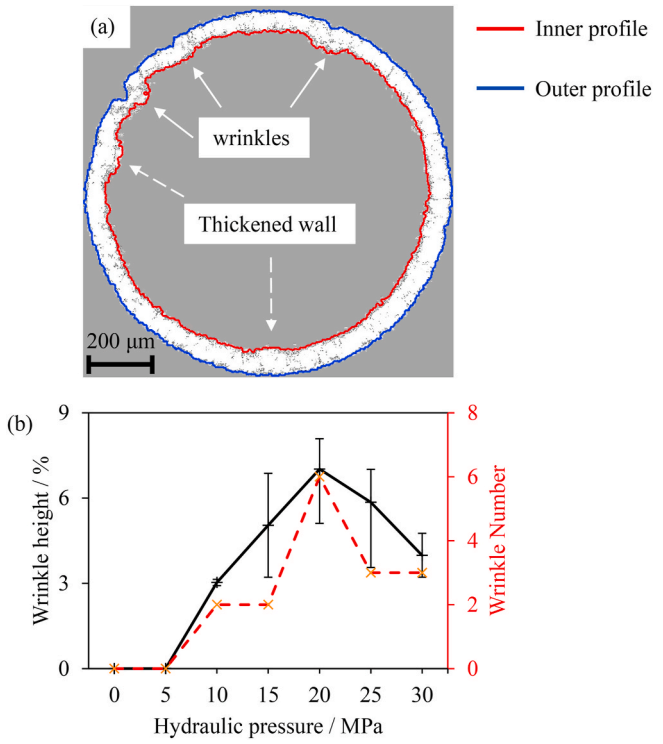

Fig. 12. (a) Recognized inner and outer profiles of a drawn cup mouth and (b) wrinkle height and number of the drawn cups.

die corner area, which increases tensile and compression stress on radial direction of the blank. This rises hydrostatic stress of the blank and reduces effective compression stress and consequent compression instability potential. Blank inhomogeneity and surface morphology result in obvious scatter of wrinkles regarding wrinkle location, height and number.

5. Conclusions

The MHDD experiments were conducted and the advanced FE model with consideration of FSI, material heterogeneity and surface morphology was developed.

Total drawing force increases with a rise of hydraulic pressure. Dual peaks of the drawing force resulted from high hydraulic pressure drawing conditions indicate wrinkles on the drawing cups, while single peak reflect a drawn cup without obvious wrinkles when drawn under low hydraulic pressures. A high pressure that greatly pre-bulges blank and affect strain-stress state of the blank will introduce wrinkles and cause dual peaks of the drawing force.

Average hydraulic pressure on the blank is lower than the inlet pressure due to leakage. Change of sealing area between the blank and die leads to different local hydraulic pressure development on the blank. MHDD tools geometry influences the hydraulic pressure development.

The maximum contact forces and contact pressures on the blank holder and die decreases with an increase of hydraulic pressure, which improves service life due to reduced wear of the MHDD tools.

Wrinkle number and height on the drawn cups increase firstly and decrease later with an increase of hydraulic pressure. This is because of integrated impacts of blank inhomogeneity, surface morphology and hydraulic pressure. The optimal hydraulic pressure in MHDD should be determined with regards to foil's characteristics including material properties and surface morphology, and MHDD tool geometry.

Declaration of competing interest

The authors declare that they have no known competing financial interests or personal relationships that could have appeared to influence the work reported in this paper.

Acknowledgement

The research is supported by the Fundamental Research Funds for the Central Universities (JZ2018HGBZ0144).

References

[1] N. Guo, J. Wang, C.Y. Sun, Y.F. Zhang, M.W. Fu, Analysis of size dependent earing evolution in micro deep drawing of TWIP steel by using crystal plasticity modeling, Int. J. Mech. Sci. 165 (2020) 105200, https://doi.org/10.1016/j.ijmecsci.2019.105200.

[2] J. Huang, Z. Xu, X. Li, L. Peng, X. Lai, An experimental study on a rapid micro imprinting process, J. Mater. Process. Technol. 283 (2020) 116716, https://doi.org/10.1016/j.jmatprotec.2020.116716.

[3] G. Behrens, F.O. Trier, H. Tetzel, F. Vollertsen, Influence of tool geometry variations on the limiting drawing ratio in micro deep drawing, Int. J. Material Form. 9 (2016) 253–258, https://doi.org/10.1007/s12289-015-1228-9.

[4] U. Engel, R. Eckstein, Microforming—from basic research to its realization, J. Mater. Process. Technol. 125–126 (2002) 35–44, https://doi.org/10.1016/S0924-0136(02)00415-6.

[5] D. Anand, D. Ravi Kumar, Effect of sheet thickness and grain size on forming limit diagrams of thin brass sheets, in: D. Deb, V.E. Balas, R. Dey (Eds.), Innovations in Infrastructure, Springer Singapore, 2019, pp. 435–444.

[6] C. Wang, B. Guo, D. Shan, Friction related size-effect in microforming – a review, Manuf. Rev. 1 (2014) 23, https://doi.org/10.1051/mfreview/2014022.

[7] U. Engel, Tribology in microforming, Wear 260 (2006) 265–273, https://doi.org/10.1016/j.wear.2005.04.021.

[8] F. Vollertsen, Categories of size effects, Prod. Eng. Res. Dev. 2 (2008) 377–383, https://doi.org/10.1007/s11740-008-0127-z.

[9] F. Vollertsen, Z. Hu, Tribological size effects in sheet metal forming measured by a strip drawing test, CIRP Ann. - Manuf. Technol. 55 (2006) 291–294, https://doi.org/10.1016/S0007-8506(07)60419-3.

[10] L. Rathmann, F. Vollertsen, Determination of a contact length dependent friction function in micro metal forming, J. Mater. Process. Technol. 286 (2020) 116831, https://doi.org/10.1016/j.jmatprotec.2020.116831.

[11] H. Sato, K. Manabe, D. Wei, Z. Jiang, S. Alexandrov, Tribological behavior in micro–sheet hydroforming, Tribol. Int. 97 (2016) 302–312, https://doi.org/10.1016/j.triboint.2016.01.041.

[12] J. Han, W. Zheng, G. Wang, M. Yu, Experimental study on size effect of dry friction in meso/micro-upsetting process, Int. J. Adv. Manuf. Technol. 95 (2018) 1127–1133, https://doi.org/10.1007/s00170-017-1291-0.

[13] H. Flosky, F. Vollertsen, Wear behaviour in a combined micro blanking and deep drawing process, CIRP Ann. - Manuf. Technol. 63 (2014) 281–284, https://doi.org/10.1016/j.cirp.2014.03.125.

[14] Z. Hu, A. Schubnov, F. Vollertsen, Tribological behaviour of DLC-films and their application in micro deep drawing, J. Mater. Process. Technol. 212 (2012) 647–652, https://doi.org/10.1016/j.jmatprotec.2011.10.012.

[15] T.C. Cheng, R.S. Lee, The influence of grain size and strain rate effects on formability of aluminium alloy sheet at high-speed forming, J. Mater. Process. Technol. 253 (2018) 134–159, https://doi.org/10.1016/j.jmatprotec.2017.10.046.

[16] H. Xie, K.-I. Manabe, Z. Jiang, Study of wire deformation characterization and size effects during the micro-flat-rolling process, Metals 10 (2020) 405, https://doi.org/10.3390/met10030405.

[17] W.L. Chan, M.W. Fu, J. Lu, J.G. Liu, Modeling of grain size effect on micro deformation behavior in micro-forming of pure copper, Mater. Sci. Eng., A 527 (2010) 6638–6648, https://doi.org/10.1016/j.msea.2010.07.009.

[18] I. Aminzahed, M.M. Mashhadi, M.R.V. Sereshk, Investigation of holder pressure and size effects in micro deep drawing of rectangular work pieces driven by piezoelectric actuator, Mater. Sci. Eng. C 71 (2017) 685–689, https://doi.org/10.1016/j.msec.2016.10.068.

[19] L. Luo, D. Wei, X. Wang, C. Zhou, Q. Huang, J. Xu, D. Wu, Z. Jiang, Effects of hydraulic pressure on wrinkling and earing in micro hydro deep drawing of SUS304 circular cups, Int. J. Adv. Manuf. Technol. 90 (2017) 189–197, https://doi.org/10.1007/s00170-016-9380-z.

[20] I. Irthiea, Experimental and numerical evaluation of micro flexible deep drawing technique using floating ring, J. Manuf. Process. 38 (2019) 556–563, https://doi.org/10.1016/j.jmapro.2019.01.050.

[21] H. Sato, K. Manabe, K. Ito, D. Wei, Z. Jiang, Development of servo-type micro-hydromechanical deep-drawing apparatus and micro deep-drawing experiments of circular cups, J. Mater. Process. Technol. 224 (2015) 233–239, https://doi.org/10.1016/j.jmatprotec.2015.05.014.

[22] R. Zafar, L. Lihui, Z. Rongjing, Analysis of hydro-mechanical deep drawing and the effects of cavity pressure on quality of simultaneously formed three-layer Al alloy parts, Int. J. Adv. Manuf. Technol. 80 (2015) 2117–2128, https://doi.org/10.1007/s00170-015-7142-y.

[23] M. Khademi, A. Gorji, M. Bakhshi, M.S. Yazdi, Investigation of wrinkling in hydrodynamic deep drawing assisted by radial pressure with inward flowing liquid, Procedia Engineering 183 (2017) 65–70, https://doi.org/10.1016/j.proeng.2017.04.012.

[24] T. Shimizu, H. Kobayashi, J. Vorholt, M. Yang, Lubrication analysis of micro-dimple textured die surface by direct observation of contact interface in sheet metal forming, Metals 9 (2019) 917, https://doi.org/10.3390/met9090917.

[25] H. Sato, K. Manabe, T. Furushima, D.B. Wei, Z.Y. Jiang, S. Alexandrov, On the scale dependence of micro hydromechanical deep drawing, Key Eng. Mater. 725 (2017) 689–694. https://doi.org/10.4028/www.scientific.net/KEM.725.689.

[26] Z. Zhang, N. Chen, T. Furushima, B. Li, Deformation behavior of metal foil in micro pneumatic deep drawing process, Procedia Manufacturing 15 (2018) 1422–1428, https://doi.org/10.1016/j.promfg.2018.07.339.

[27] H. Kamali, H. Xie, H. Zhao, F. Jia, H. Wu, Z. Jiang, Frictional size effect of light-weight Mg–Li alloy in micro deep drawing under nano-particle lubrication condition, Mater. Trans. 61 (2020) 239–243, https://doi.org/10.2320/matertrans.MT-ML2019002.

[28] Z. Xu, L. Peng, P. Yi, X. Lai, An investigation on the formability of sheet metals in the micro/meso scale hydroforming process, Int. J. Mech. Sci. 150 (2019) 265–276, https://doi.org/10.1016/j.ijmecsci.2018.10.033.

[29] H. Sato, K. Manabe, D. Wei, Z. Jiang, D. Kondo, Micro Sheet Hydroforming Process of Ultra-thin Pure Titanium Foil, Faculty of Engineering and Information Sciences - Papers, 2015, pp. 397–401. https://doi.org/10.4028/www.scientific.net/KEM.626.397.

[30] L. Luo, Z. Jiang, D. Wei, X. Wang, C. Zhou, Q. Huang, Micro-hydromechanical deep drawing of metal cups with hydraulic pressure effects, Front. Mech. Eng. 13 (2018) 66–73, https://doi.org/10.1007/s11465-018-0468-z.

[31] F. Barlat, K. Lian, Plastic behavior and stretchability of sheet metals. Part I: a yield function for orthotropic sheets under plane stress conditions, Int. J. Plast. 5 (1989) 51–66, https://doi.org/10.1016/0749-6419(89)90019-3.

[32] N. Aquelet, ALE adaptive mesh refinement in LS-DYNA, 2012, pp. 1–20, https://www.dynamore.de/de/download/papers/2012-internationale-ls-dyna-users-conference/documents/fsi-ale23-a.pdf. (Accessed 5 June 2016).

[33] H.N. Lu, D.B. Wei, Z.Y. Jiang, X.H. Liu, K. Manabe, Modelling of size effects in microforming process with consideration of grained heterogeneity, Comput. Mater. Sci. 77 (2013) 44–52. https://doi.org/10.1016/j.commatsci.2013.03.033.